

On the Nature of Type Ia-CSM Supernovae: Optical and Near-Infrared Spectra of SN 2012ca and SN 2013dn

Ori D. Fox^{1,2}, Jeffrey M. Silverman³, Alexei V. Filippenko¹, Jon Mauerhan¹,
Juliette Becker⁴, H. Jacob Borish⁵, S. Bradley Cenko^{6,7}, Kelsey I. Clubb¹, Melissa Graham¹,
Eric Hsiao^{8,9}, Patrick L. Kelly¹, William H. Lee¹⁰, G. H. Marion³, Dan Milisavljevic¹¹,
Jerod Parrent¹¹, Isaac Shivvers¹, Michael Skrutskie⁵, Nathan Smith¹², John Wilson⁵,
and Weikang Zheng¹

¹*Department of Astronomy, University of California, Berkeley, CA 94720-3411, USA.*

²*ofox@berkeley.edu.*

³*Department of Astronomy, University of Texas at Austin, Austin, TX 78712, USA.*

⁴*Cahill Center for Astrophysics, California Institute of Technology, Pasadena, CA 91125, USA.*

⁵*Department of Astronomy, University of Virginia, P.O. Box 400325, Charlottesville, VA 22904-4325, USA.*

⁶*Astrophysics Science Division, NASA Goddard Space Flight Center, MC 661, Greenbelt, MD 20771, USA.*

⁷*Joint Space-Science Institute, University of Maryland, College Park, MD 20742, USA.*

⁸*Carnegie Institution of Washington, Las Campanas Observatory, Colina El Pino, Casilla 601, Chile.*

⁹*Department of Physics and Astronomy, Aarhus University, Ny Munkegade, DK-8000 Aarhus C, Denmark.*

¹⁰*Instituto de Astronomía, Universidad Nacional Autónoma de México, Apartado Postal 70-264, 04510 México D.F., Mexico.*

¹¹*Harvard-Smithsonian Center for Astrophysics, 60 Garden St., Cambridge, MA 02138, USA.*

¹²*Steward Observatory, University of Arizona, 933 North Cherry Avenue, Tucson, AZ 85721, USA.*

28 August 2014

ABSTRACT

A growing subset of Type Ia supernovae (SNe Ia) show evidence for unexpected interaction with a dense circumstellar medium (SNe Ia-CSM). The precise nature of the progenitor, however, remains debated owing to spectral ambiguities arising from a strong contribution from the CSM interaction. Late-time spectra offer potential insight if the post-shock cold, dense shell becomes sufficiently thin and/or the ejecta begin to cross the reverse shock. To date, few high-quality spectra of this kind exist. Here we report on the late-time optical and infrared spectra of the SNe Ia-CSM 2012ca and 2013dn. These SNe Ia-CSM spectra exhibit low $[\text{Fe III}]/[\text{Fe II}]$ ratios and strong $[\text{Ca II}]$ at late epochs. Such characteristics are reminiscent of the super-Chandrasekhar-mass (SC) candidate SN 2009dc, for which these features suggested a low-ionisation state due to high densities, although the broad Fe features admittedly show similarities to the blue “quasi-continuum” observed in some core-collapse SNe Ibn and IIn. Neither SN 2012ca nor any of the other SNe Ia-CSM show evidence for broad oxygen, carbon, or magnesium in their spectra. Similar to the interacting Type IIn SN 2005ip, a number of high-ionisation lines are identified in SN 2012ca, including $[\text{S III}]$, $[\text{Ar III}]$, $[\text{Ar X}]$, $[\text{Fe VIII}]$, $[\text{Fe X}]$, and possibly $[\text{Fe XI}]$. The total bolometric energy output does not exceed 10^{51} erg, but does require a large kinetic-to-radiative conversion efficiency. All of these observations taken together suggest that SNe Ia-CSM are more consistent with a thermonuclear explosion than a core-collapse event, although detailed radiative transfer models are certainly necessary to confirm these results.

Key words: circumstellar matter — supernovae: general — supernovae: individual (SN 1997cy, SN 1988Z, SN 1998S, SN 2002ic, SN 2005gj, SN 2005ip, SN 2006jc, SN 2007gr, SN 2008J, SN 2009dc, SN 2009ip, SN 2010jl, SN 2011hw, PTF11kx, SN 2012ca, SN 2013cj, SN 2013dn, SN 2014J)

1 INTRODUCTION

Type Ia supernovae (SNe Ia; see Filippenko 1997 for a review) are attributed to the thermonuclear explosion of a C/O white dwarf (WD) primary star that approaches the Chandrasekhar limit by accreting material from a companion star. While the nature of the companion remains somewhat ambiguous, recent arguments suggest that a WD companion (i.e., a double-degenerate progenitor) is more commonplace than the single-degenerate scenario (see Maoz et al. 2013 for a review). Given that these highly evolved stars have long since shed their outer envelopes, the surrounding circumstellar medium (CSM) is expected to have a relatively low density. In fact, the lack of a significant CSM is one of the primary reasons SNe Ia can be used as precise cosmological distance indicators (e.g., Phillips 1993).

A growing number of SNe Ia, however, show evidence of interaction with a dense CSM during the first year post-explosion, and sometimes longer (Silverman et al. 2013b, and references within). Classified as SNe Ia-CSM, the spectra have Type Ia features (e.g., S II and Si II absorption lines) near maximum light that are weaker than usual, most likely diluted by a strong continuum (e.g., Leloudas et al. 2013). The spectra also have relatively narrow hydrogen emission lines, which arise from the dense and slowly moving CSM formed by pre-SN mass loss that is more typically associated with core-collapse SNe II_n (Schlegel 1990; Filippenko 1997). These dense environments suggest that either (a) single-degenerate progenitor scenarios are responsible for these explosions, or (b) the exploding star was not a thermonuclear explosion of a white dwarf at all.

The SN Ia-CSM progenitor explosion mechanism (i.e., thermonuclear versus core collapse) remains debated in the literature (e.g., Inserra et al. 2014). For example, the two most well-studied SN Ia-CSM templates (SNe 2002ic and PTF11kx) were classified as SNe Ia at early times, showing a resemblance to the overluminous SN 1991T (Hamuy et al. 2003; Deng et al. 2004; Wood-Vasey et al. 2004; Dilday et al. 2012; Silverman et al. 2013a). Compared to SNe II_n, weaker and narrower He, H β , and O lines in SNe Ia-CSM further support arguments for a thermonuclear origin (Silverman et al. 2013b). For this case of a thermonuclear explosion, Hamuy et al. (2003) propose the dense CSM may be attributed to an evolved secondary star (i.e., single-degenerate binary progenitor).

Alternatively, other SNe Ia-CSM show less obvious S or Si at early times (e.g., SNe 1997cy and 2005gj), but are only classified as SNe Ia-CSM because later spectra exhibit iron features and/or match SNe 2002ic and PTF11kx very well (e.g., Germany et al. 2000; Aldering et al. 2006). Benetti et al. (2006) argue for a core-collapse origin instead, given that some SNe Ic (e.g., SN 2004aw) can be confused for SNe Ia at early phases if considering only similarities of 6300 Å features most often attributed to Si II λ 6355. Furthermore, Inserra et al. (2014) make line identifications of intermediate/heavy elements in the spectra of the SN Ia-CSM 2012ca that are consistent with a core-collapse explosion of an evolved massive star. The ambiguity is compounded by the fact that the available catalogs of SN Ia spectra already suggest a number of degeneracies in the spectroscopic classification process (see Parrent et al. 2014 for a review). Furthermore, spectroscopic models of ther-

Table 1. Summary of Distances to Reported SNe Ia-CSM

SN	Distance (Mpc)	Reference
2014ab	95	ATel 4076
2014T	375	CBET 3815
2014Y	162	CBET 3824
2013dn	233	CBET 3570
2013I	144	CBET 3386
2012ca	79	CBET 3101
CSS120327:110520-015205	215	ATel 4081
2011dz	100	CBET 2761
2011jb	142	CBET 2947
PTF11kx	194	Dilday et al. 2012
PTF10htz	147	Silverman et al. 2013b
2009in	98	CBET 1953
2008J	92	CBET 1218

monuclear SNe with CSM interaction (CSI) have not yet been constructed. Owing to the strong CSI and underlying continuum, even post-photospheric phase spectra may offer little evidence about the ejecta composition to connect with the pre-maximum spectral type and the related progenitor system (Leloudas et al. 2013).

SN 2012ca stands out as being one of the most nearby SNe Ia-CSM (79 Mpc; see Table 1), allowing for high-resolution data having a high signal-to-noise ratio (S/N), even at late times after the CSI has faded and the ejecta begin to cross the reverse shock. Here we present new optical and infrared (IR) spectra of SN 2012ca, along with a number of other SNe Ia-CSM, SNe II_n, and SNe Ia. We compare the line identifications of Inserra et al. (2014) among the various spectra in our database. In particular, we consider the case of the SN Ia-CSM 2013dn, for which we have well-sampled, high-S/N spectra through day \sim 441 post-maximum. Section 2 presents the observations, while §3 offers a detailed comparison of the spectra to other SN types. In §4 we discuss the implications on the SN Ia-CSM progenitor, and §5 summarises our conclusions.

2 OBSERVATIONS

This paper presents new data on SNe Ia-CSM 2012ca and 2013dn and SNe II_n 2005ip and 2009ip. SN 2012ca was discovered in the late-type spiral galaxy ESO 336-G009 on 2012 Apr. 25.6 (UT dates are used throughout this paper) at redshift $z = 0.019$ ($m_r \approx 14.8$ mag; Drescher et al. 2012; Inserra et al. 2014). The earliest spectrum matches that of SN Ia-CSM 1997cy at an estimated ~ 60 days post-maximum (Inserra et al. 2012; Valenti et al. 2012), although the peak of SN 1997cy was never observed (Germany et al. 2000; Turatto et al. 2000). Similar to Inserra et al. (2014), we take the light-curve peak to be 2012 Mar. 2.

SN 2013dn was discovered in the galaxy PGC 71942 on 2013 Jun. 14.45 at $z = 0.056$ ($m_r \approx 16.2$ mag; Drake et al. 2013). The earliest spectrum (2013 Jun. 26.13) matches that of SN Ia-CSM 2005gj at 54 days post-explosion (Drake et al. 2013), although at this redshift the derived absolute magnitude (~ -21.1) is somewhat brighter than that derived for SN 2005gj around maximum light. Given that SN 2005gj peaks ~ 32 days post-explosion in the r (Prieto et al. 2007),

Table 2. RATIR Photometry of SN 2013dn

JD – 2,450,000	Epoch (days)	<i>r</i>	<i>i</i>	<i>Z</i>	<i>Y</i>	<i>J</i>	<i>H</i>	Log $L_{\text{opt}}/(\text{erg s}^{-1})$
					mag			
6510	106	17.00 (0.02)	17.01 (0.02)	16.61 (0.02)	16.78 (0.03)	17.16 (0.03)	17.18 (0.04)	43.12
6519	115	17.25 (0.02)	17.01 (0.02)	16.74 (0.02)	16.92 (0.03)	17.37 (0.03)	17.26 (0.04)	43.39
6539	135	17.30 (0.02)	17.20 (0.02)	16.93 (0.02)	17.08 (0.03)	17.56 (0.06)	17.44 (0.08)	43.29
6546	142	17.48 (0.02)	17.40 (0.02)	17.06 (0.02)	17.21 (0.03)	–	–	43.26
6551	147	17.42 (0.02)	17.34 (0.02)	16.96 (0.02)	17.25 (0.03)	17.77 (0.05)	17.59 (0.08)	43.23
6562	158	17.53 (0.02)	17.43 (0.02)	17.03 (0.02)	17.29 (0.03)	17.86 (0.05)	17.75 (0.07)	43.20
6579	175	17.85 (0.02)	17.61 (0.02)	17.15 (0.03)	17.54 (0.04)	18.13 (0.05)	17.98 (0.08)	43.11
6591	187	18.04 (0.02)	17.73 (0.02)	17.21 (0.02)	17.72 (0.04)	18.10 (0.05)	18.11 (0.08)	43.09
6606	202	17.99 (0.02)	17.88 (0.02)	17.34 (0.02)	17.98 (0.04)	18.35 (0.06)	18.44 (0.09)	43.02
6612	208	18.01 (0.02)	17.90 (0.02)	17.93 (0.03)	18.09 (0.04)	18.30 (0.06)	18.21 (0.09)	42.98
6621	217	18.11 (0.02)	18.03 (0.02)	17.47 (0.03)	18.18 (0.04)	18.44 (0.06)	18.72 (0.09)	42.95
6632	228	18.16 (0.02)	18.08 (0.02)	17.51 (0.03)	18.31 (0.04)	18.48 (0.06)	18.77 (0.09)	42.94
6638	234	18.30 (0.02)	18.21 (0.02)	17.62 (0.03)	18.27 (0.04)	18.60 (0.06)	18.71 (0.09)	42.89
6680	276	18.57 (0.02)	18.46 (0.02)	17.90 (0.03)	18.59 (0.04)	18.07 (0.09)	18.13 (0.19)	42.81
6821	417	19.95 (0.03)	19.97 (0.04)	19.49 (0.05)	–	>19.00	>18.75	42.26

we take 2013 Jun. 4 to be the *r*-band light-curve peak for SN 2013dn.

SN 2005ip was discovered in NGC 2906 on 2005 Nov. 5 at $z = 0.0072$ (Boles et al. 2005), although early-time optical spectra suggested the discovery occurred a few weeks following the explosion (Modjaz et al. 2005). The spectra, dominated by narrow hydrogen emission lines, led to a Type IIn classification (Fox et al. 2009; Smith et al. 2009). While there are no precise constraints on the explosion date, Smith et al. (2009) and Fox et al. (2009) suggest the peak may have been ~ 2 weeks prior to the discovery. We therefore take 2005 Oct. 22 for the light-curve peak.

SN 2009ip was originally classified as a SN (Maza et al. 2009), but was actually discovered during a luminous blue variable star (LBV) outburst and did not undergo its most extreme outburst until 2012 August (Mauerhan et al. 2013; Fraser et al. 2013a,b; Pastorello et al. 2013; Prieto et al. 2013; Smith et al. 2013, 2014; Graham et al. 2014; Levesque et al. 2014; Margutti et al. 2014). The progenitor has not been confirmed to have disappeared, but evidence suggests the star underwent a terminal explosion (Mauerhan et al. 2014; Smith et al. 2014). The progenitor was probably a massive star (i.e., not a white dwarf), given (1) high and continuous pre-SN wind speeds ($> 600 \text{ km s}^{-1}$), (2) a luminous ($10^6 L_{\odot}$) and eruptive progenitor (Smith et al. 2010), and (3) the presence of a hot LBV spectrum during the earlier “impostor” phases (Smith et al. 2010; Foley et al. 2011; Pastorello et al. 2013). Similar to Smith et al. (2014), we take the light-curve peak to be 2012 Sep. 24.

All epochs presented in this article correspond to days post-maximum unless otherwise specified.

2.1 Optical and Near-Infrared Photometry

Photometry of SN 2013dn was obtained with the multi-channel Reionization And Transients InfraRed camera (RATIR; Butler et al. 2012) mounted on the 1.5-m Johnson telescope at the Mexican Observatorio Astronómico Nacional on Sierra San Pedro Mártir in Baja California, México (Watson et al. 2012). Typical observations include a series

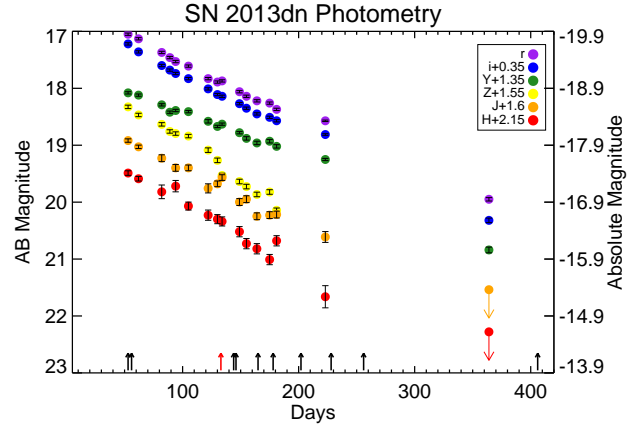


Figure 1. Optical/IR light curve of SN 2013dn. Black arrows signify epochs at which optical spectra were obtained. The red arrow marks the epoch at which the near-IR spectrum was obtained.

of 80-s exposures in the *ri* bands and 60-s exposures in the *ZYJH* bands, with dithering between exposures. RATIR’s fixed IR filters cover half of their respective detectors, automatically providing off-target IR sky exposures while the target is observed in the neighbouring filter. Master IR sky frames are created from a median stack of off-target images in each IR filter. No off-target sky frames were obtained on the optical CCDs, but the small galaxy size and sufficient dithering allowed for a sky frame to be created from a median stack of all the images in each filter. Flat-field frames consist of evening sky exposures. Given the lack of a cold shutter in RATIR’s design, IR dark frames are not available. Laboratory testing, however, confirms that the dark current is negligible in both IR detectors (Fox et al. 2012).

The data were reduced, coadded, and analysed using standard CCD and IR processing techniques in IDL and Python, utilising online astrometry programs **SExtractor** and **SWarp**¹. Calibration was performed using field stars with

¹ **SExtractor** and **SWarp** can be accessed from <http://www.astromatic.net/software>.

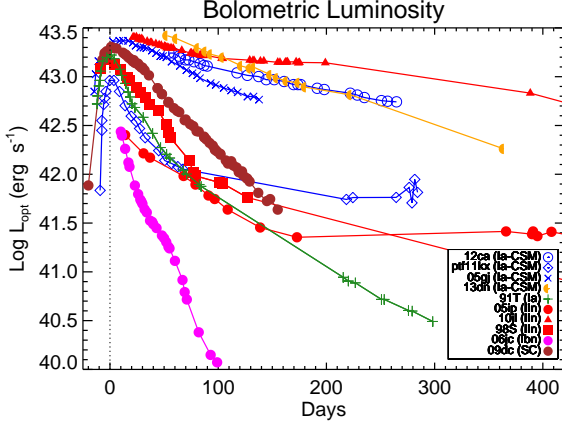


Figure 2. Bolometric light curve of SN 2013dn (orange) compared to that of several well-known SNe IIn (red), SNe Ia-CSM (blue), and the overluminous Type Ia SN 1991T (green). Although both the SNe Ia-CSM and SNe IIn have late-time light-curve plateaus caused by ongoing CSI, the peak and plateau luminosities can vary significantly within each class. The total radiated luminosity output for SN 2013dn (and several other SNe Ia-CSM) is similar to that of some of the SNe IIn ($\sim \text{few} \times 10^{50}$ erg), which is still consistent with a thermonuclear explosion of a white dwarf ($\sim 10^{51}$ erg) but requires a high conversion efficiency (~ 0.5).

reported fluxes in both 2MASS (Skrutskie et al. 2006) and the Sloan Digital Sky Survey (SDSS) Data Release 9 Catalogue (Ahn et al. 2012). Figure 1 plots (and Table 2 lists) the optical and near-IR photometry obtained for SN 2013dn. For a comparison, Figure 2 plots the bolometric luminosity against that of other relevant SNe we will be comparing.

2.2 Optical Spectroscopy

Table 3 summarises the details concerning new optical spectra presented in this paper. Figure 3 plots all the spectra of SNe 2013dn. Some data were obtained with the Kast double spectrograph on the Shane 3-m telescope at Lick Observatory (Miller & Stone 1993), the dual-arm Low Resolution Imaging Spectrometer (LRIS; Oke et al. 1995) mounted on the 10-m Keck I telescope, and the DEep Imaging Multi-Object Spectrograph (DEIMOS; Faber et al. 2003) on the 10-m Keck II telescope. Most observations had the slit aligned along the parallactic angle to minimise differential light losses (Filippenko 1982).

Additional spectra were obtained with the Hiltner 2.4 m telescope at MDM Observatory using the Boller & Chivens CCDS spectrograph.² The 150 line mm^{-1} grating was used with a $1.2''$ slit to yield spectra having a full width at half-maximum intensity (FWHM) resolution of 12 \AA . Data were also obtained from the MMT 6.5-m telescope using the Blue Channel (BC) spectrograph (Schmidt et al. 1989). The 300 and 1200 line mm^{-1} gratings were used in conjunction with a $1.0''$ slit to yield spectra having FWHM resolutions of 7 and 2 \AA , respectively.

The spectra were reduced using standard techniques (e.g., Foley et al. 2003; Silverman et al. 2012b). Routine CCD processing and spectrum extraction were completed

² <http://www.astronomy.ohio-state.edu/MDM/CCDS/>.

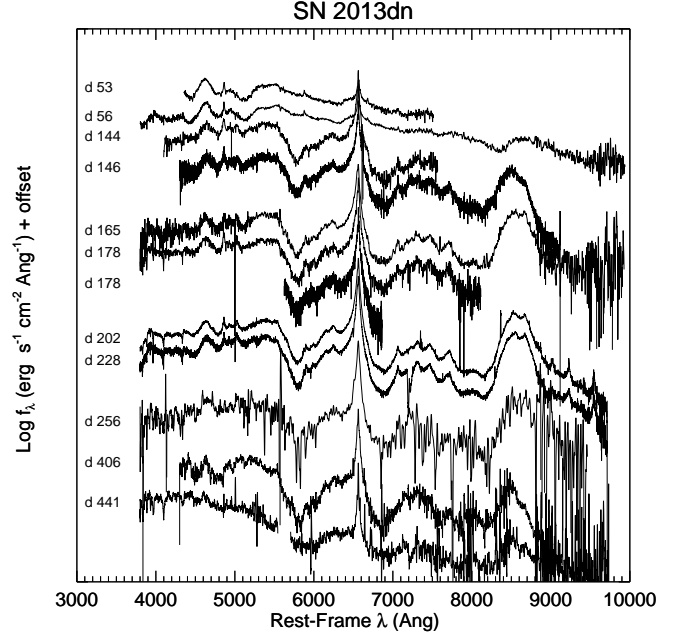


Figure 3. Time series of optical spectra of the Type Ia-CSM SN 2013dn.

Table 3. Summary of Optical Spectra

SN	JD – 2,450,000	Epoch (days)	Instrument	Int (s)
2013dn	6479	53	MDM/MkIII	2700
	6482	56	Lick/Kast	900
	6570	144	MDM/CCDS	3600
	6572	146	Keck/DEIMOS	2400
	6591	165	Lick/Kast	2400
	6604	178	MMT/BC-300	1200
	6604	178	MMT/BC-1200	2400
	6628	202	Keck/LRIS	2400
	6654	228	Keck/DEIMOS	2400
	6682	256	Lick/Kast	2400
2012ca	6834	406	Keck/DEIMOS	1200
	6834	441	Keck/LRIS	1200
2009ip	6484	502	Keck/DEIMOS	600
	6506	524	Keck/DEIMOS	600

with IRAF³, and the data were extracted with the optimal algorithm of Horne (1986). We obtained the wavelength scale from low-order polynomial fits to calibration-lamp spectra. Small wavelength shifts were then applied to the data after cross-correlating a template-sky spectrum to an extracted night-sky spectrum. Using our own IDL routines, we fit a spectrophotometric standard-star spectrum to the data in

³ IRAF: the Image Reduction and Analysis Facility is distributed by the National Optical Astronomy Observatory, which is operated by the Association of Universities for Research in Astronomy (AURA), Inc., under cooperative agreement with the US National Science Foundation (NSF).

Table 4. Summary of Infrared Spectra

SN	JD – 2,450,000	Epoch (days)	Instrument
2014J	6727	36	TripleSpec (APO)
	6786	95	TripleSpec (APO)
2013dn	6559	133	TripleSpec (APO)
2012ca	6053	70	FIRE
	6087	104	FIRE
2010jl	5657	170	TripleSpec (APO)
	6727	1233	TripleSpec (APO)
2005ip	4547	884	TripleSpec (APO)
	4580	917	TripleSpec (APO)
	6727	3064	TripleSpec (APO)
2008J	4714	234	TripleSpec (APO)
2007gr	4376	35	TripleSpec (Palomar)
	4450	109	FIRE

order to flux calibrate the SN and to remove telluric absorption lines (Wade & Horne 1988; Matheson et al. 2000).

Other optical spectra used throughout this paper were obtained from both the Berkeley Supernova Database (Silverman et al. 2012b) and the Weizmann Interactive Supernova data REpository (WiSeRep; Yaron & Gal-Yam 2012).

2.3 Near-Infrared Spectroscopy

Table 4 summarises the details concerning new near-IR spectra presented in this paper. Some data were obtained with TripleSpec spectrographs (Wilson et al. 2004; Herter et al. 2008) operating at both the Apache Point Observatory 3-m and the Palomar Observatory 5-m telescopes. TripleSpec observations typically consisted of 300-s exposures, taken at varying locations along the slit and then pair-subtracted to allow for the correction of night-sky emission lines. We extract the spectra with a modified version of the IDL-based *SpecTool* (Cushing et al. 2004). The underlying galaxy and sky emission are approximated by a polynomial fit and subtracted from the supernova. A-type calibration stars were observed directly after each SN exposure to remove telluric absorption lines using the IDL-based *xtellcor* package (Vacca et al. 2003). The day +917 of SN 2010jl was previously published by Borish et al. (2014), along with the full near-IR evolution of SN 2005ip from earlier epochs.

Other IR spectra were obtained with the Folded-port InfraRed Echellette (FIRE) spectrograph at the Magellan 6.5-m telescope (Simcoe et al. 2008). The FIRE spectra were obtained in the high-throughput prism mode with a $0''.6$ slit. This configuration yields a continuous wavelength coverage from 0.8 to 2.5 μm with a resolution of $R \approx 500$ in the J band. When acquiring the supernova, the slit was oriented at the parallactic angle to minimise the effect of atmospheric dispersion (Filippenko 1982). At each epoch, several frames were obtained using the conventional ABBA “nod-along-the-slit” technique and the “sampling-up-the-ramp” read-out mode. The per-frame exposure time was between 95.1 and 158.5 s, depending on the brightness of the supernova.

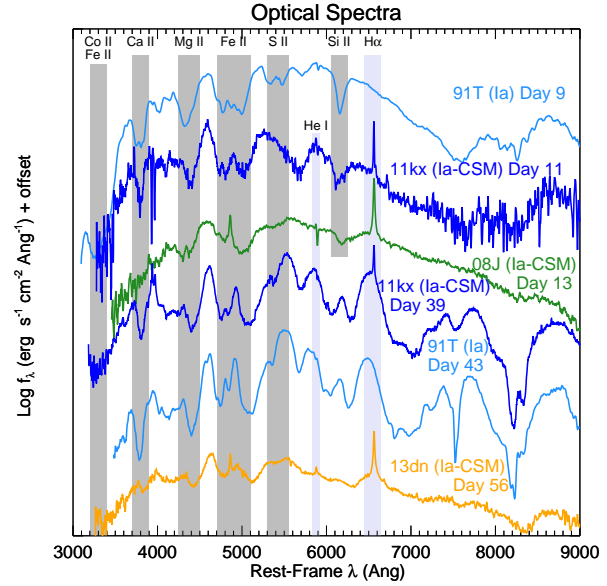


Figure 4. Comparison of early-time spectra, including the Type Ia SN 1991T (light blue), the Type Ia-CSM PTF11kx (dark blue), the Type IIn/Ia-CSM SN 2008J (green), and the Type Ia-CSM SN 2013dn (orange). Vertical grey bars highlight the position of several broad absorption lines associated with SNe Ia, while vertical light-blue bars highlight the position of narrow H and He emission associated with SNe IIn. SN 2013dn looks very similar to SN 2008J, which was decomposed into a combination of a SN 1991T-like event and a blackbody continuum (Taddia et al. 2012).

These exposure times were chosen such that adequate signal was obtained in each frame without saturating the bright night-sky lines in the K band. At each epoch, an A0V star was observed close to the science observations in time, angular distance, and airmass for telluric correction, as per the method described by Vacca et al. (2003).

The data were reduced using the IDL pipeline *firehose*, specifically designed for the reduction of FIRE data. The pipeline performed steps of flat fielding, wavelength calibration, sky subtraction, spectral tracing, and spectral extraction. The sky flux was modeled using off-source pixels as described by Kelson (2003) and subtracted from each frame. Next, the spectral extraction was performed using the optimal technique (Horne 1986), a weighting scheme that delivers the maximum S/N while preserving spectrophotometric accuracy. Individual spectra were then combined with sigma clipping to reject spurious pixels. Corrections for telluric absorption were performed using the IDL tool *xtellcor* developed by Vacca et al. (2003). To construct a telluric correction spectrum free of stellar absorption features, a model spectrum of Vega was used to match and remove the hydrogen lines of the Paschen and Brackett series from the A0V telluric standard. The resulting telluric correction spectrum was also used for flux calibration.

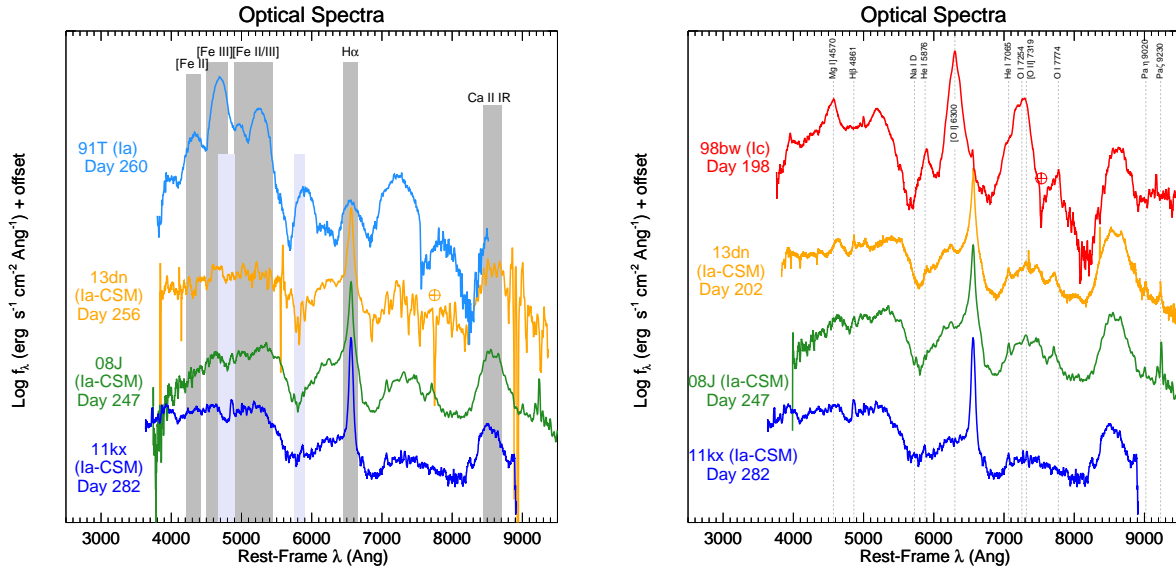


Figure 5. (left) Comparison of late-time spectra, including the Type Ia SN 1991T (light blue), the Type Ia-CSM PTF11kx (dark blue), the Type II_n/Ia-CSM SN 2008J (green), the Type Ia-CSM SN 2013dn (orange). (right) Comparison of the interacting SNe Ia-CSM to the broad-lined Type Ic SN 1998bw (red). Dashed vertical grey lines highlight several of the more prominent narrow features, solid grey vertical bars mark a few of the broader features, and solid blue vertical bars show some of the more prominent P Cygni features. Not all lines appear in all spectra. Also note that the 6500 Å feature in SN 1991T is a blend of [Fe II] and Co, not H α .

3 ANALYSIS OF THE SPECTRA

3.1 Early-Time Optical Spectra

Figure 4 illustrates the early-time evolution of several SNe ranging from days +9 to 56, including the SNe Ia-CSM 2013dn (orange), 2008J (green), and PTF11kx (dark blue), and the overluminous SN Ia 1991T (light blue). Owing to difficulties in identifying and removing the continuum, we instead apply a minimal degree of artificial reddening or dereddening for plotting purposes in Figure 4. This reddening/dereddening does not change the presence of any spectral lines and is not applied during the analysis of the spectra elsewhere in the article (although we deredden SN 2008J throughout the paper by a factor consistent with measurements of Taddia et al. (2012)). Vertical grey bars highlight the position of several broad absorption lines associated with SNe Ia, while vertical light blue bars mark the position of narrow H and He emission associated with SNe II_n. At these early times, the overall blue colour of the spectra is caused by the continuum from the underlying photosphere.

SN 1991T (day +9) exhibits the deepest absorption lines, but this spectrum was also obtained closest to peak brightness. Even so, SN 1991T-like objects tend to have weaker lines than do normal SNe Ia or underluminous SNe Ia (e.g., SN 1991bg; Silverman et al. 2012a). The corresponding absorption lines are still noticeable in SNe Ia-CSM, particularly PTF11kx, despite being weakened by the underlying continuum and H/He emission lines. Earlier spectra of SN 2008J have even more pronounced absorption features and can be decomposed into a combination of a SN 1991T-like event and a blackbody continuum (Taddia et al. 2012). The earliest spectrum we obtained of SN 2013dn was on day +56, but even at this epoch the spectrum shows remarkable similarity to SN 2008J on day +13. Furthermore, despite the

varying degrees of underlying continuum and the S/N, these two SNe share many of the same features as PTF11kx.

3.2 Late-Time Optical Spectra

Figure 5 compares the SNe Ia-CSM at later epochs, ranging from days +202 to 282. We also consider the Type Ia SN 1991T (light blue) and the broad-lined Type Ic SN 1998bw (red) given their widespread use in other papers (e.g., Inserra et al. 2014). The reader should be aware, however, of several conditions that make a direct comparison difficult. First, strong circumstellar lines and an underlying continuum dominate the spectra of the interacting SNe, but are not necessarily associated with the exploding star or ejecta. A cold, dense shell (CDS) can form between the forward and reverse shocks that, if optically thick, may further obscure the underlying ejecta. Second, the continuum levels are difficult to identify since the blue flux shortward of 5500 Å in the SNe Ia-CSM may arise from a “quasi-continuum” produced by many overlapping permitted and forbidden lines of iron-group elements (e.g., Deng et al. 2004; Bowers et al. 1997; Branch et al. 2008; Silverman et al. 2013b). Third, the nebular spectra of SNe Ia do not have many unique or unambiguous characteristic features among various SN Ia subtypes (see Fig. 13 of Parrent et al. 2014). We discuss the implications of these effects on our interpretation in §4.

Figure 6 compares different SN types on a linear scale over different epochs at late-times. The linear scale highlights the relative line intensities more clearly than the log scale in Figure 5. All spectra are scaled by a multiplicative factor to highlight features relative to the likely continuum, which we identify as being just redward of H α (~ 6800 Å) and just blueward of He I $\lambda 5876$. The SNe Ia-CSM have three distinguishing traits: (1) a low [Fe III] $\lambda 4700$ /[Fe II]

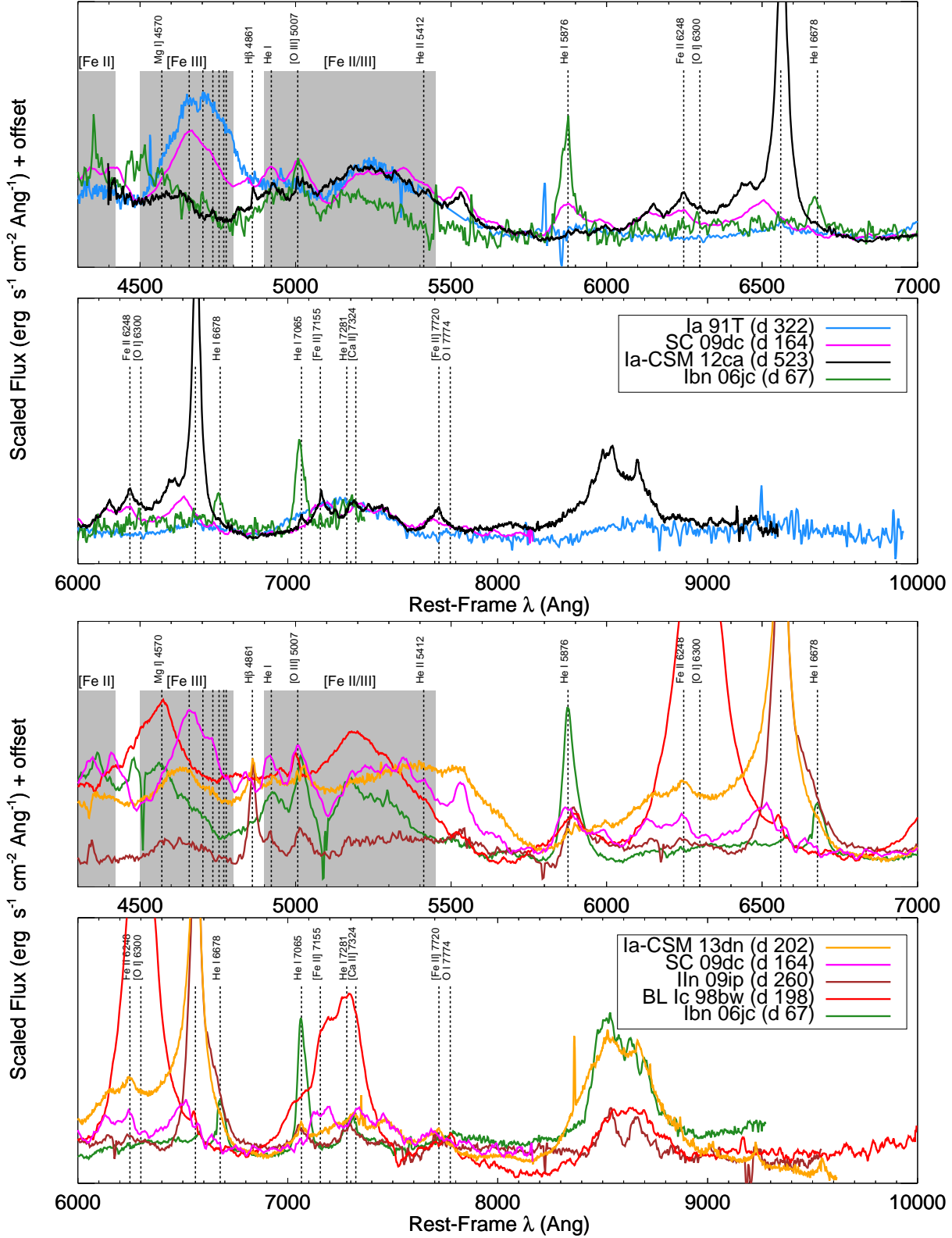


Figure 6. (top) Comparison of SN 2012ca (black) at later epochs to the Type Ia SN 199T (light blue), the super-Chandrasekhar-mass (CS) candidate Type Ia SN 2009dc (pink), and the Type Ibn SN 2006jc (green). (bottom) Comparison of SN 2013dn (orange) at ~ 200 days to the CS candidate Type Ia SN 2009dc (pink), the Type IIn SN 2009ip (brown), the Type Ibn SN 2006jc (green), and the broad-lined Type Ic SN 1998bw (red). Dashed vertical lines highlight several of the more prominent narrow features, while solid grey vertical bars mark a few of the broader iron features. Unlabeled dotted black lines correspond to [Fe III].

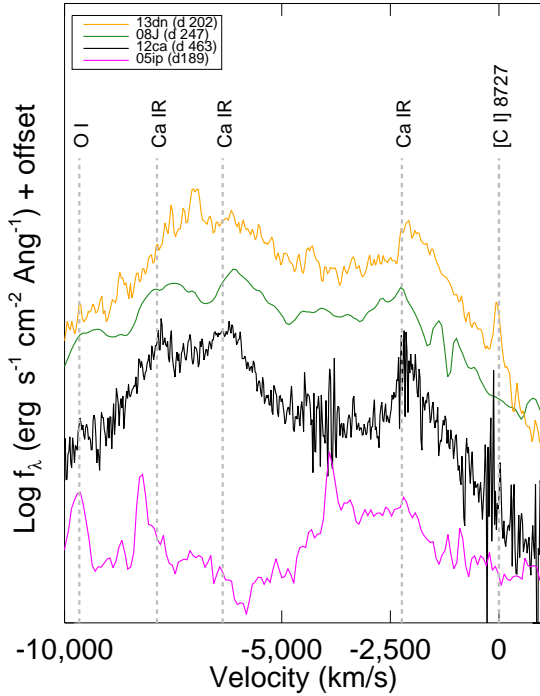


Figure 9. Velocity profiles of spectra plotted in Figure 7, plus the Type IIn/Ia-CSM SN 2008J (green). Vertical grey dashed lines mark the primary carbon line at rest velocity. At a blueshift of $\sim 2500 \text{ km s}^{-1}$, a line consistent with Ca II exists. This line, in fact, is the dominant line identified in the spectra presented by Inserra et al. (2012). Some carbon does exist, however, in SNe 2013dn and 2012ca, but not in the Type IIn SN 2005ip.

be consistent with blueshifted oxygen actually correspond to broad iron lines that we describe in §3.2.3 below. Nonetheless, we note that all of the spectra do show evidence for weaker and unshifted O I $\lambda 7774$, [O I] $\lambda 6300$, and O I $\lambda 8446$ with FWHM $\approx 1000 \text{ km s}^{-1}$.

Carbon: Inserra et al. (2014) also identify the [C I] $\lambda 8727$ line after day +256. Figure 7 again marks this line both in the rest frame (grey) and blueshifted (blue). Figure 9 plots the velocity profiles for SNe 2005ip, 2012ca, 2008J, and 2013dn. If the carbon were expected to be found in the ejecta, like the oxygen, then we would should see a -2500 km s^{-1} shift. Indeed, there is an emission feature at -2500 km s^{-1} , but this line is consistent with the Ca IR triplet. We do detect emission at $\sim 0 \text{ km s}^{-1}$ in SNe 2012ca and 2013dn, but this line is (1) at 0 km s^{-1} and (2) narrow, both of which would be unexpected if associated with the blueshifted ejecta.

3.2.3 High-Ionisation Coronal Lines

Section 3.2.2 suggests alternate line identifications for the blueshifted oxygen. Compared to SN 2005ip (Smith et al. 2009), Figure 8 shows that [Fe II] emission corresponds to the wavelengths at these blueshifts. Smith et al. (2009) identify a number of other forbidden iron and relatively high-ionisation lines in SN 2005ip, many of which are more commonly associated with the solar corona (coronal lines; e.g., Wagner & House 1968), active galactic nuclei (AGNs; e.g., Filippenko 1989), and novae (e.g., Williams et al. 1991), but

are rare in SNe. Smith et al. (2009) point out that no other SN has exhibited such a variety of narrow coronal lines, aside from a few of the stronger ones in SNe IIn 1988Z and 1995N (Turatto et al. 1993; Fransson et al. 2002), although a number of these lines are also observed in nearby SN remnants (Fesen & Hurford 1996).

Figure 10 compares SNe Ia-CSM 2012ca (black) and 2013dn (orange) to SNe IIn 2005ip (pink) and 2009ip (brown). Using line lists made for SN 2005ip (Smith et al. 2009) and nearby supernova remnants (Fesen & Hurford 1996), we identify a number of high-ionisation lines in SNe 2012ca and 2009ip (also see Table 5), including [S III], [Ar III], [Ar X], [Fe VIII], [Fe X], and possibly [Fe XI], although all lines are not quite as prominent in the SNe Ia-CSM as they are in SN 2005ip. The lines we detect generally correspond to the strongest coronal lines in SN 2005ip, since the underlying continuum likely overwhelms the presences of the weaker lines.

Smith et al. (2009) attribute the narrow ($\sim 120\text{--}240 \text{ km s}^{-1}$) coronal lines in SN 2005ip to pre-shock ionisation of the CSM by sustained X-ray emission from ongoing CSI. The ionisation potentials imply high temperatures up to $\sim 2 \times 10^6 \text{ K}$. Smith et al. (2009) go on to explain the lack of any higher-velocity components in these lines with a clumpy or asymmetric CSM, which can arise from various progenitor systems with evolved stars and do not necessarily distinguish between a core-collapse and thermonuclear explosion. Dense clumps can decelerate the forward shock, giving rise to intermediate-width H α lines, but also leading to efficient cooling and suppression of coronal lines in the post-shock cooling region. At the same time, the X-rays generated by the CSI can escape along paths without clumps to ionise the pre-shock CSM.

3.3 Near-Infrared Line Identifications

Figure 11 compares the near-IR spectra of the Type IIn/Ia-CSM SN 2008J (green), the Type Ia-CSM SN 2013dn (orange), the Type Ia-CSM SN 2012ca (black), the Type Ic SN 2007gr (red), the Type IIn SN 2010jl (brown), the Type Ia SN 2014J (dark blue), and the Type IIn SN 2005ip (pink). We identify spectral features from line lists previously compiled for some well-sampled near-IR spectra, including those of the Type Ic SN 2007gr (Hunter et al. 2009), the Type IIn SN 1998S (Fassia et al. 2001), and the Marion et al. (2009) Type Ia sample (see also Table 6). Not all lines appear in all spectra. While the underlying continuum from CSI again makes comparisons difficult, we discuss the primary features below.

H: Both the SNe Ia-CSM and SNe IIn near-IR spectra have numerous hydrogen lines. The more prominent Paschen and Brackett lines are identified throughout the spectrum. Like other SNe IIn, the line widths of a few thousand km s^{-1} are consistent with CSM swept up by the forward shock.

Helium: A line at $\sim 1.0830 \mu\text{m}$ is detected in SNe 2007gr, 2013dn, 2008J, 2012ca, 2010jl, and 2005ip. This line is commonly associated with He, but it can be easily confused with Si I $\lambda 10827$. In fact, Hunter et al. (2009) attribute this feature in SN 2007gr to a combination of He I, Si I, and Mg II, while the large absorption trough at $\sim 1.04 \mu\text{m}$ is attributed to C I. Furthermore, at a width of $\sim 10^4 \text{ km s}^{-1}$,

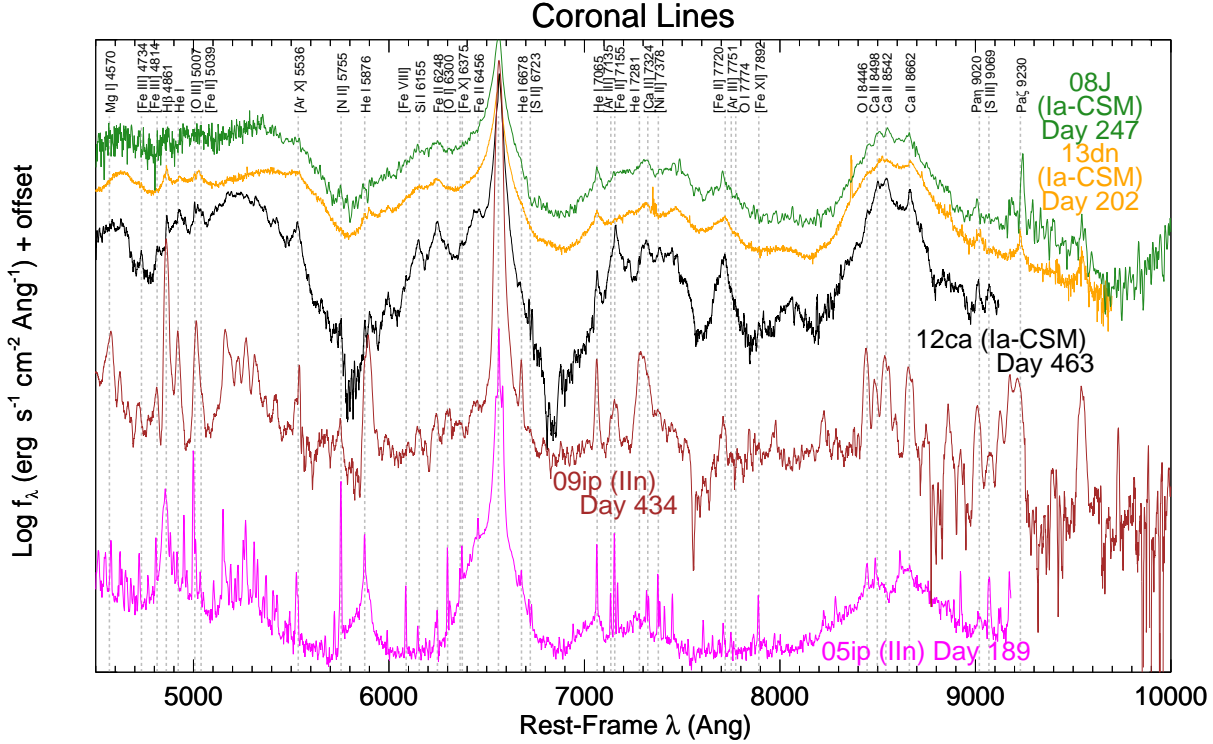


Figure 10. Comparison of late-time spectra, including the Type IIn/Ia-CSM SN 2008J (green), the Type Ia-CSM SN 2013dn (orange), the Type Ia-CSM SN 2012ca (black), the Type IIn SN 2009ip (brown), and the Type IIn SN 2005ip (pink). Some of high-ionisation coronal lines originally identified in SN 2005ip are seen in a number of SNe Ia-CSM and listed in Table 5.

Table 5. Optical Line Identifications

λ (Å)	Line	λ (Å)	Line
4733.93	[Fe III]	7065.19	He I
4813.9	[Fe III]	7135.80	[Ar III]
4861.36	H β	7155.14	[Fe II]
4921.93	He I	7281.35	He I
5039.10	[Fe II]	7323.88	[Ca II]
5536	[Ar X]	7377.83	[Ni II]
5754.59	[Ni II]	7719.9	[Fe II]
5876 blend	He I	7751.06	[Ar III]
6087.90	[Fe VIII]	7774 blend	O I
6155	Si I	7891.80	[Fe XI]
6247.56	Fe II	8498.02	Ca II
6374.51	[Fe X]	8542.09	Ca II
6456.38	Fe II	8662.14	Ca II
6560	H α	9020	Pa η
6678.15	He I	9069.0	[S III]
6723	[S II]	9230	Pa ζ

the line is heavily blended with Pa γ , and the red wing of the feature bleeds into the blue wing of O I (Borish et al. 2014).

A more clearly defined He line is at 2.0589 μm (Modjaz et al. 2009). A broad line at this wavelength is also detected in SNe 2013dn, 2008J, 2012ca, 2010jl, and 2005ip, but not in SN 2007gr. In fact, He is also detected in the optical spectra at 7065 Å. Although Silverman et al. (2013b) note little or no He I emission in their SN Ia-CSM sample, their spectra were obtained at earlier epochs when still

dominated by an underlying continuum. Regardless, we see no reason for He to distinguish between a thermonuclear or core-collapse event. The He, which has similar velocities as the H lines, likely originated in the progenitor system’s wind and was accelerated by the forward shock. A number of scenarios can produce a He wind in the years leading up to the white dwarf explosion (e.g., Lundqvist et al. 2013).

Mg I: Inserra et al. (2014) identify Mg I $\lambda\lambda$ 11,300, 15,024, which they use to argue for a core-collapse explosion. Indeed, these lines (along with Mg I $\lambda\lambda$ 17,109) are prominent in the Type Ic SN 2007gr. However, the Mg I $\lambda\lambda$ 15,024, 17,109 lines are not detected in any of the SNe Ia-CSM or SN 2010jl, and the Mg I λ 11,300 line is relatively weak, if detected at all. Furthermore, the 1.1300 μm line identification can be easily confused with O I λ 1.1287 μm , which we find is more precisely aligned with the features apparent in SNe 2012ca and 2008J. Compared to Type IIn SNe 2010jl and 2005ip, these lines are more narrow, which likely suggest that they do not originate in the ejecta. Weakening of the apparent line strength by a strong, underlying continuum must be considered, but the Mg I lines are some of the strongest lines observed in the Type Ic SN 2007gr and should still be observed in the interacting SNe if present. Furthermore, Figure 6 (bottom) shows a clear detection of Mg I λ 4570 in the nebular spectra of SN 1998bw, but not in the SNe Ia-CSM. Broad emission features near this wavelength may be confused with Mg, but are more likely the suppressed [Fe III] discussed in §3.1.

Oxygen: Several oxygen lines also reside in the near-IR, including O I $\lambda\lambda$ 11,287, 13,165 and O II λ 21,085. As

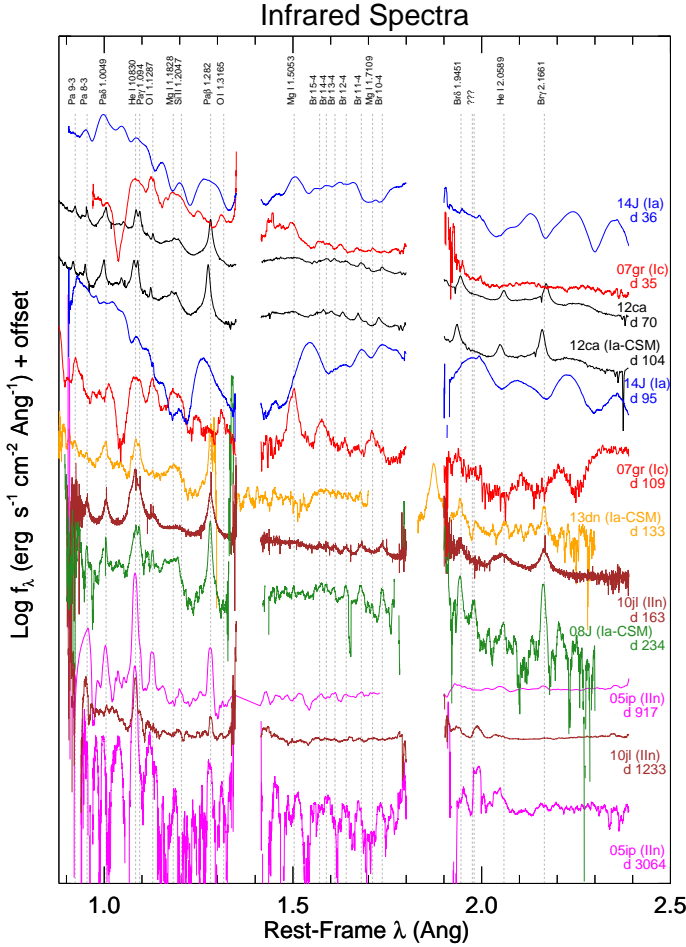


Figure 11. Comparison of IR spectra, including the Type IIn/Ia-CSM SN 2008J (green), the Type Ia-CSM SN 2013dn (orange), the Type Ia-CSM SN 2012ca (black), the Type Ic SN 2007gr (red), the Type IIn SN 2010jl (brown), the Type Ia SN 2014J (dark blue), and the Type IIn SN 2005ip (pink).

expected, these lines are prominently detected in SN 2007gr. If the 1.1287 μm line is O I (as we suggest above), it is significantly weaker in SN 2012ca, 2008J, and 2013dn than in SN 2007gr. This line, however, most likely has contributions from other elements anyway. A small detection at 1.3165 μm is observed in the day +66 spectrum of SN 2012ca, but this might be from the surrounding CSM and is certainly not persistent. No O I λ 13,165 or O II λ 21,085 is detected in SNe 2012ca, 2008J, 2013dn, or even 2010jl. Furthermore, none of these lines requires a blueshift like that described for the optical spectra of SN 2012ca. Nonetheless, it should be noted that these near-IR spectra are still dominated by shock-related emission and do not adequately probe nebular lines from the ejecta. The spectrum of SN 2005ip on day +3064, which clearly shows the emergence of broad nebular oxygen lines, underscores this point.

Table 6. Infrared Line Identifications

λ (μm)	Line	λ (μm)	Line
0.92315	Pa 9-3	1.5053	Mg I
0.95486	Pa 8-3	1.5705	Br 15-4
1.0049	P δ	1.5885	Br 14-4
1.0830	He I	1.6114	Br 13-4
1.0938	P γ	1.6412	Br 12-4
1.1287	O I	1.6811	Br 11-4
1.1828	Mg I	1.7109	Mg I
1.2047	Mg I	1.7367	Br 10-4
1.2818	P β	1.9451	Br δ
1.3165	O I	2.1661	Br γ

4 DISCUSSION

4.1 Source of the Emission at Late Times

To interpret the spectra first requires identification of the spectral line origins in the physical SN environment. Figure 2 shows that some of the SNe Ia-CSM and SNe IIn can be a factor of 100 more luminous than even SN 1991T at late times. The normal radioactively powered nebular phase of the underlying thermonuclear explosion can therefore only contribute $< 5\%$ of the total flux at these epochs. The majority of the luminosity is instead powered by CSI (and so using the word “nebular” is not quite appropriate even at these late epochs).

While the luminosity may be dominated by CSI, the ejecta need not be completely obscured by an opaque shell. The CSM in many of these systems is likely asymmetric (e.g., Mauerhan et al. 2014). The CDS also continues to expand and can become optically thin over time. Reprocessing of X-rays and ultraviolet (UV) light generated by the shock interaction can illuminate the ejecta to observable levels. Furthermore, the ejecta will be excited as they cross the reverse shock at late epochs (e.g., Mauerhan & Smith 2012).

Any differences between the spectral lines of normal SNe Ia and SNe Ia-CSM/IIn may therefore be caused by any combination of the following reasons. (1) Stratification of the composition and/or ionisation of the ejecta, since they are illuminated from the outside-in, not from the inside-out. (2) The source of heat is thermalised UV and X-rays or the crossing of the reverse shock, but not gamma rays from radioactivity, which could also have a strong impact on the ionisation stratification of the ejecta. (3) Inherent differences in the explosion type and ejecta composition. Radiative transfer models can provide a more definitive answer, but they are beyond the scope of this paper.

4.2 [Fe III] and the Blue “Quasi-Continuum”

The broad [Fe III] and [Fe II] highlighted in Figure 6, often referred to as a blue “quasi-continuum,” is composed of blended iron-group elements (e.g., Foley et al. 2007; Smith et al. 2009, 2012). Silverman et al. (2013b) point to this quasi-continuum in favour of a thermonuclear origin despite weak [Fe III] when compared to most nebular SNe Ia (e.g., SN 1991T). We note, however, that weak [Fe III] has been observed previously in other SNe Ia. Here we refer to the case of SC candidate SN 2009dc, which was believed to have resulted from the explosion of a WD exceeding the

Chandrasekhar limit due to high rotation velocities (and also modeled as a “tamped detonation” due to merging white dwarfs by Raskin et al. 2014). SN 2009dc showed suppressed [Fe III].

Figure 6 highlights the similarities SN 2009dc (pink) shares with the SNe Ia-CSM (aside from H α of course). In fact, the [Fe III] emission is still stronger in SN 2009dc than in the SNe Ia-CSM (particularly on day +164), but significantly less than in the overluminous SN 1991T. Taubenberger et al. (2013) attribute the smaller [Fe III]/[Fe II] ratio in SN 2009dc to a low-ionisation state during the nebular phase owing to high central ejecta densities (and therefore, enhanced recombination). In the case of SN 2009dc, these high densities may be a result of the low ejecta expansion velocities observed in SC SNe (e.g., Silverman et al. 2011; Taubenberger et al. 2011), whereas for the SNe Ia-CSM the high densities likely result from decelerated ejecta by the dense CSM. Taubenberger et al. (2013) go on to show that the low-ionisation state would also be consistent with the detection of [Ca II] $\lambda\lambda 7291, 7324$, since the first and second ionisation potentials of Ca are lower than those of iron. Indeed, Figure 6 shows that [Ca II] is detected in both the SC and SNe Ia-CSM.

Admittedly, such a blue “quasi-continuum” has also been observed in other interacting SNe, including the SNe Ibn 2006jc (Foley et al. 2007) and 2011hw (Smith et al. 2012) and the SN IIn 2005ip (Smith et al. 2009). As described for the cases of SNe Ibn 2006jc and 2011hw (Smith et al. 2012), which have lost a majority of their H envelopes, a low H abundance will place the burden of the radiative cooling from the CSI on the Fe emission lines. In other words, the Fe lines may very well originate in the ejecta, but the strength of the lines *may* be an indicator of the H, rather than the Fe, abundance.

Figure 6 compares the SNe Ia-CSM 2013dn (orange) and 2012ca (black) to the SN Ibn 2006jc (green), the SN IIn 2009ip (brown), and the SC SN 2009dc (pink). While there are some similarities in the shapes of the “quasi-continuum,” there are several important differences to the overall spectra. First, the hydrogen features in SNe 2013dn and 2012ca are significantly stronger than those in SN 2006jc, suggesting that the H abundance is not particularly low in the SNe Ia-CSM. The H line strength may not directly indicate the total gas mass, but the light curves in Figure 2 show that the luminosity from CSM interaction is significantly stronger and more extended in SNe 2012ca and 2013dn than in either SN 2006jc or SN 2005ip. The total mass of gas, composed primarily of H, is therefore larger in these SNe Ia-CSM. Second, the [Fe III] lines are present in SNe 2013dn and 2009dc, and even identifiable in SN 2012ca, but seemingly absent in SN 2006jc. Third, the Mg I $\lambda 4570$ feature in SN 1998bw is detected in SN 2006jc, but not in SNe 2009dc, 2013dn, or 2012ca. We are surely limited by the epochs of data we have to compare SN 2009dc to SN 2012ca since the [Fe III] becomes only more suppressed over time in SN 2009dc.

4.3 The Nature of the Type Ia-CSM Progenitor

Inserra et al. (2014) suggest the SNe Ia-CSM match well with SN 1998bw, but we find this comparison difficult to reconcile with our data. Namely, [O I] $\lambda 6300$ in SN 1998bw is too strong (as is [Ca II]), particularly considering we do

not detect any significant oxygen in our SN Ia-CSM spectra (see §3.2.2). We also do not detect any carbon or magnesium. The SNe Ia CSM feature at $\sim 4600\text{--}4700$ Å is more likely suppressed [Fe III] than the Mg I found in SN 1998bw. The weak [Fe III] and strong [Ca II] in the nebular spectra of the SNe Ia-CSM are most similar to the SC SN 2009dc, which was modeled by a low-ionisation state owing to high densities that we would also expect in the SNe Ia-CSM.

Furthermore, Figure 2 shows the bolometric light curve of several SNe Ia-CSM. All SN Ia-CSM peak magnitudes are > -19 , and the total integrated radiated luminosity output is a few $\times 10^{50}$ erg, which is still consistent with a thermonuclear explosion of a white dwarf ($\sim 10^{51}$ erg) but requires a high conversion efficiency of kinetic energy into radiation ($\epsilon \approx 0.5$). While such conversion efficiencies are quite high, they are certainly possible (e.g., van Marle et al. 2010). The Type Ia IR signatures are less apparent.

With a thermonuclear progenitor in mind, we reconsider Figure 10, which highlights strong iron lines (e.g., $\lambda\lambda 6248, 7155, 7720$) in the spectra of SNe 2012ca, 2009ip, 2013dn, and 2008J. Figures 8 plots the velocity profiles for these iron lines. Compared to SN 2005ip, both the SNe Ia-CSM and the SN IIn 2009ip have broader line profiles (≥ 1000 km s $^{-1}$). If associated with the pre-shock wind, as suggested in the case of SN 2005ip, the higher velocities could potentially imply progenitor scenarios that differ from the massive-star progenitors with low speed winds (i.e., LBVs) proposed for most SNe IIn. These velocities, however, are not consistent with the more narrow hydrogen and helium (≤ 1000 km s $^{-1}$; see Figure 12), which are associated with the pre-shock CSM. Instead, these broad iron lines more likely originate in the post-shock cooling region or in the ejecta, which would be more consistent with SNe Ia.

The broad iron lines in SN 2009ip may be surprising given it has a progenitor that has most certainly been identified as a massive star (i.e., core collapse; see §2). Of course, X-rays produced by the CSI may excite even solar abundances of iron in post-shock CSM. In this case, these iron features would not be a useful discriminator. Furthermore, Figure 6 (bottom) compares a day +260 spectrum of the interacting Type IIn SN 2009ip (brown) to the SNe Ia-CSM. While SN 2009ip does exhibit some evidence for iron emission shortward of 5500 Å, it is significantly weaker than the other thermonuclear events. This fact alone is an important differentiator between the SNe IIn and SNe Ia-CSM in our sample.

Despite our discussion about the oxygen misidentifications in §3.2.2, we note that we do detect some oxygen $\lambda\lambda 5007, 6300, 8446$ in the nebular spectra of both SNe Ia-CSM 2013dn, 2012ca and SNe IIn 2009ip, 2005ip. The oxygen emission, however, is relatively weak and narrow, and the broader lines at 8446 Å are more likely a result of Ly α pumping (which scales linearly with density) and not recombination. In this case, the lack of intermediate-mass elements in SN 2009ip and 2005ip may be more of the surprise. These results have been used to argue against a terminal core collapse in SN 2009ip already (Fraser et al. 2013b), but Smith et al. (2014) point out that even their late-time spectra were dominated by CSI. Even if the ejecta are illuminated, the illumination comes from the outside shocks and the intermediate-mass elements may be hidden deep in the ejecta or the lines may be weak. Indeed, the lack of nu-

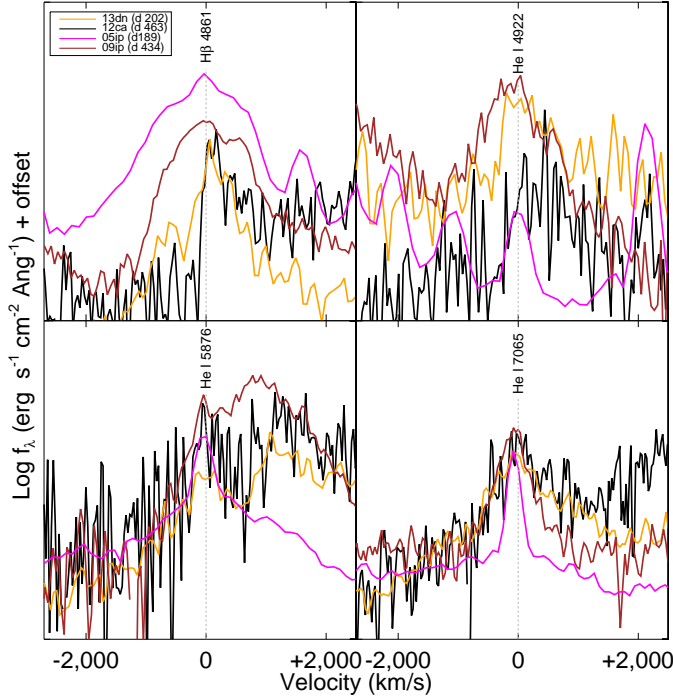


Figure 12. Velocity profiles of several H/He lines, including the Type Ia-CSM SN 2013dn (orange), the Type Ia-CSM SN 2012ca (black), the Type IIn SN 2009ip (brown), and the Type IIn SN 2005ip (pink). Vertical dashed lines identify prominent spectral lines, although it should be noted that not all lines appear in all spectra.

cleosynthetic signatures in SNe IIn is a common trait (e.g., SNe 2005ip and 1998S) that results from the formation of an optically thick shell from CSI that obscures emission from the ejecta (Mauerhan & Smith 2012). Late-time spectra of SNe IIn only begin to show evidence for broad oxygen emission if the ejecta are still bright enough once the CSI sufficiently fades and/or the ejecta begin to cross the reverse shock. Therefore, this comparison may be less relevant than previously suggested.

5 CONCLUSIONS AND FUTURE WORK

We find the SN Ia-CSM subclass to be more consistent with a thermonuclear explosion than a core-collapse event. Specifically, the spectra do not showing evidence for intermediate-mass elements and do exhibit broad iron features, a low $[\text{Fe III}]/[\text{Fe II}]$ ratio most similar to the super-Chandrasekhar-mass candidate SN 2009dc, and a total bolometric energy output that does not exceed 10^{51} erg. Nonetheless, there is still some ambiguity as to the origin of the blue “quasi-continuum.” Larger samples comparing these features as a function of bolometric luminosity and hydrogen line strength will be necessary to further disentangle the origin of the quasi-continuum. This work also highlights the need for robust radiative transfer models for comparison.

While the case for a thermonuclear origin appears to have gained a more robust foothold, the companion’s properties still remain relatively unknown. Furthermore, the

ability for the companion to undergo such high mass loss (i.e., $> 10^{-3} M_{\odot}$; see Silverman et al. 2013b, and references therein) remains poorly understood, although the presence of a binary likely has a role (e.g., Smith & Tombleson 2014). Future multi-wavelength observations will be needed to probe the CSM characteristics, trace the CSI, constrain the progenitor mass-loss history, and identify late-time heating mechanisms of warm dust.

Insightful discussions were shared with many at the Aspen Center for Physics, including Ryan Foley, Ryan Chornock, and Craig Wheeler. This work was supported in part by NSF Grant No. PHYS-1066293 and the hospitality of the Aspen Center for Physics. Some of the data presented herein were obtained at the W. M. Keck Observatory, which is operated as a scientific partnership among the California Institute of Technology, the University of California, and NASA; the observatory was made possible by the generous financial support of the W. M. Keck Foundation. We are grateful to the staffs of the Lick and Keck Observatory for their assistance with the observations, and thank the RATIR instrument team and the staff of the Observatorio Astronómico Nacional on Sierra San Pedro Mártir. RATIR is a collaboration between the University of California, the Universidad Nacional Autónoma de México, NASA Goddard Space Flight Center, and Arizona State University, benefiting from the loan of an H2RG detector from Teledyne Scientific and Imaging. RATIR, the automation of the Harold L. Johnson Telescope of the Observatorio Astronómico Nacional on Sierra San Pedro Mártir, and the operation of both are funded by the partner institutions and through NASA grants NNX09AH71G, NNX09AT02G, NNX10AI27G, and NNX12AE66G, CONACyT grant INFR-2009-01-122785, UNAM PAPIIT grant IN113810, and a UC MEXUS-CONACyT grant. J.M.S. is supported by an NSF Astronomy and Astrophysics Postdoctoral Fellowship under award AST-1302771. A.V.F.’s supernova group at UC Berkeley received support through NSF grant AST-1211916, the TABASGO Foundation, Gary and Cynthia Bengier, the Richard and Rhoda Goldman Fund, and the Christopher R. Redlich Fund.

REFERENCES

- Ahn, C. P., Alexandroff, R., Prieto, C. A., et al. 2012, *ApJS*, 203, 21
- Aldering, G., Antilogus, P., Bailey, S., et al. 2006, *ApJ*, 650, 510
- Benetti, S., Cappellaro, E., Turatto, M., et al. 2006, *ApJL*, 653, L129
- Boles, T., Nakano, S., & Itagaki, K. 2005, *CBET*, 275, 1
- Borish, H. J., Huang, C., Chevalier, R. A., et al. 2014, *arXiv: 1406.5531*
- Bowers, E. J. C., Meikle, W. P. S., Geballe, T. R., et al. 1997, *MNRAS*, 290, 663
- Branch, D., Jeffery, D. J., Parrent, J., et al. 2008, *PASP*, 120, 135
- Butler, N., Klein, C., Fox, O., et al. 2012, *Proc. of the SPIE*, 8446, 10
- Cushing, M. C., Vacca, W. D., & Rayner, J. T. 2004, *PASP*, 116, 362

- Deng, J., Kawabata, K. S., Ohyama, Y., et al. 2004, *ApJ*, 605, L37
- Dilday, B., Howell, D. A., Cenko, S. B., et al. 2012, *Science*, 337, 942
- Drake, A. J., Djorgovski, S. G., Graham, M. J., et al. 2013, *CBET*, 3570, 1
- Drescher, C., Parker, S., & Brimacombe, J. 2012, *CBET*, 3101, 1
- Faber, S. M., Phillips, A. C., Kibrick, R. I., et al. 2003, *Proc. of SPIE*, 4841, 1657
- Fassia, A., Meikle, W. P. S., Chugai, N., et al. 2001, *MNRAS*, 325, 907
- Fesen, R. A., & Hurford, A. P. 1996, *ApJS*, 106, 563
- Filippenko, A. V. 1982, *PASP*, 94, 715
- . 1989, *AJ*, 97, 726
- . 1997, *ARA&A*, 35, 309
- Foley, R. J., Berger, E., Fox, O., et al. 2011, *ApJ*, 732, 32
- Foley, R. J., Smith, N., Ganeshalingam, M., et al. 2007, *ApJ*, 657, L105
- Foley, R. J., Papenkova, M. S., Swift, B. J., et al. 2003, *PASP*, 115, 1220
- Fox, O. D., Skrutskie, M. F., Chevalier, R. A., et al. 2009, *ApJ*, 691, 650
- Fox, O. D., Kutyrev, A. S., Rapchun, D. A., et al. 2012, *Proc. of SPIE*, 8453, 59
- Fransson, C., Chevalier, R. A., Filippenko, A. V., et al. 2002, *ApJ*, 572, 350
- Fraser, M., Kotak, R., Pastorello, A., et al. 2013a, *ATEL*, 4953, 1
- Fraser, M., Inserra, C., Jerkstrand, A., et al. 2013b, *MNRAS*, 433, 1312
- Germany, L. M., Reiss, D. J., Sadler, E. M., Schmidt, B. P., & Stubbs, C. W. 2000, *ApJ*, 533, 320
- Graham, M. L., Sand, D. J., Valenti, S., et al. 2014, *ApJ*, 787, 163
- Hamuy, M., Phillips, M. M., Suntzeff, N. B., et al. 2003, *Nature*, 424, 651
- Herter, T. L., Henderson, C. P., Wilson, J. C., et al. 2008, *Proc. of SPIE*, 7014, 30
- Horne, K. 1986, *PASP*, 98, 609
- Hunter, D. J., Valenti, S., Kotak, R., et al. 2009, *A&A*, 508, 371
- Inserra, C., Smartt, S. J., Valenti, S., et al. 2012, *CBET*, 3101, 2
- Inserra, C., Smartt, S. J., Scalzo, R., et al. 2014, *MNRAS Letters*, 437, L51
- Kelson, D. D. 2003, *PASP*, 115, 688
- Leloudas, G., Hsiao, E. Y., Johansson, J., et al. 2013, *arXiv:1306.1549*, 1306, 1549
- Levesque, E. M., Stringfellow, G. S., Ginsburg, A. G., Bally, J., & Keeney, B. A. 2014, *AJ*, 147, 23
- Lundqvist, P., Mattila, S., Sollerman, J., et al. 2013, *MNRAS*, 435, 329
- Maoz, D., Mannucci, F., & Nelemans, G. 2013, *arXiv:1312.0628*
- Margutti, R., Milisavljevic, D., Soderberg, A. M., et al. 2014, *ApJ*, 780, 21
- Marion, G. H., Höflich, P., Gerardy, C. L., et al. 2009, *AJ*, 138, 727
- Matheson, T., Filippenko, A. V., Ho, L. C., Barth, A. J., & Leonard, D. C. 2000, *AJ*, 120, 1499
- Mauerhan, J., & Smith, N. 2012, *MNRAS*, 424, 2659
- Mauerhan, J., Williams, G. G., Smith, N., et al. 2014, *MNRAS*, 442, 1166
- Mauerhan, J. C., Smith, N., Filippenko, A. V., et al. 2013, *MNRAS*, 749
- Maza, J., Hamuy, M., Antezana, R., et al. 2009, *CBET*, 1928, 1
- Milisavljevic, D., Fesen, R., Chevalier, R., et al. 2012, *ApJ*, 751, 25
- Miller, J. S., & Stone, R. P. S. 1993, *Lick Obs. Tech. Rep.*, 66
- Modjaz, M., Kirshner, R., Challis, P., & Calkins, M. 2005, *IAU Circ.*, 8628, 2
- Modjaz, M., Li, W., Butler, N., et al. 2009, *ApJ*, 702, 226
- Oke, J. B., Cohen, J. G., Carr, M., et al. 1995, *PASP*, 107, 375
- Parrent, J., Friesen, B., & Parthasarathy, M. 2014, *Ap&SS*, 351, 1
- Pastorello, A., Cappellaro, E., Inserra, C., et al. 2013, *ApJ*, 767, 1
- Phillips, M. M. 1993, *ApJ*, 413, L105
- Prieto, J. L., Brimacombe, J., Drake, A. J., & Howerton, S. 2013, *ApJL*, 763, L27
- Prieto, J. L., Garnavich, P. M., Phillips, M. M., et al. 2007, *eprint arXiv*, 0706, 4088, 63 pages, 16 figures, submitted to *AJ*
- Raskin, C., Kasen, D., Moll, R., Schwab, J., & Woosley, S. 2014, *ApJ*, 788, 75
- Schlegel, E. M. 1990, *MNRAS*, 244, 269
- Schmidt, G. D., Weymann, R. J., & Foltz, C. B. 1989, *PASP*, 101, 713
- Silverman, J. M., Ganeshalingam, M., Li, W., et al. 2011, *MNRAS*, 410, 585
- Silverman, J. M., Kong, J. J., & Filippenko, A. V. 2012a, *MNRAS*, 425, 1819
- Silverman, J. M., Foley, R. J., Filippenko, A. V., et al. 2012b, *MNRAS*, 425, 1789
- Silverman, J. M., Nugent, P. E., Gal-Yam, A., et al. 2013a, *ApJ*, 772, 125
- . 2013b, *ApJS*, 207, 3
- Simcoe, R. A., Burgasser, A. J., Bernstein, R. A., et al. 2008, *Proc. of SPIE*, 7014, 0
- Skrutskie, M. F., Cutri, R. M., Stiening, R., et al. 2006, *AJ*, 131, 1163
- Smith, N., Mauerhan, J. C., Kasliwal, M. M., & Burgasser, A. J. 2013, *MNRAS*, 434, 2721
- Smith, N., Mauerhan, J. C., & Prieto, J. L. 2014, *MNRAS*, 438, 1191
- Smith, N., Mauerhan, J. C., Silverman, J. M., et al. 2012, *MNRAS*, 426, 1905
- Smith, N., & Tombleson, R. 2014, *arXiv*: 1406.7431
- Smith, N., Silverman, J. M., Chornock, R., et al. 2009, *ApJ*, 695, 1334
- Smith, N., Miller, A., Li, W., et al. 2010, *AJ*, 139, 1451
- Taddia, F., Stritzinger, M. D., Phillips, M. M., et al. 2012, *A&A*, 545, L7
- Taubenberger, S., Benetti, S., Childress, M., et al. 2011, *MNRAS*, 412, 2735
- Taubenberger, S., Kromer, M., Hachinger, S., et al. 2013, *MNRAS*, 432, 3117
- Turatto, M., Cappellaro, E., Danziger, I. J., et al. 1993, *MNRAS*, 262, 128
- Turatto, M., Mazzali, P. A., Suzuki, T., et al. 2000, *Super-*

- novae and gamma-ray bursts: The Greatest Explosions Since the Big Bang: poster papers from the Space Telescope Science Institute Symposium, 72
- Vacca, W. D., Cushing, M. C., & Rayner, J. T. 2003, The Publications of the Astronomical Society of the Pacific, 115, 389
- Valenti, S., Pastorello, A., Cappellaro, E., et al. 2012, ATEL, 4076, 1
- van Marle, A. J., Smith, N., Owocki, S. P., & van Veelen, B. 2010, MNRAS, 407, 2305
- Wade, R. A., & Horne, K. 1988, ApJ, 324, 411
- Wagner, W. J., & House, L. L. 1968, Solar Physics, 5, 55
- Watson, A. M., Richer, M. G., Bloom, J. S., et al. 2012, Proc. of SPIE, 8444, doi:10.1117/12.926927
- Williams, R. E., Hamuy, M., Phillips, M. M., et al. 1991, ApJ, 376, 721
- Wilson, J. C., Henderson, C. P., Herter, T. L., et al. 2004, Proc. of SPIE, 5492, 1295
- Wood-Vasey, W. M., Wang, L., & Aldering, G. 2004, ApJ, 616, 339
- Yaron, O., & Gal-Yam, A. 2012, PASP, 124, 668